RSC Advances

PAPER

View Article Online
View Journal | View Issue

Cite this: *RSC Adv.*, 2021, **11**, 18938

Structural insights into targeting of the colchicine binding site by ELR510444 and parbendazole to achieve rational drug design†

Jia-Hong Lei,‡[a] Ling-Ling Ma,‡[b] Jing-Hong Xian,[c] Hai Chen,[b] Jian-Jian Zhou,[d] Hao Chen,[e] Qian Lei,[b] Yu-Yan Li,[ab] Yan-Yan Wang*[f] and Yu-Xi Wang *[ab]

Received 13th February 2021
Accepted 27th April 2021

DOI: 10.1039/d1ra01173a

rsc.li/rsc-advances

Microtubules consisting of α- and β-tubulin heterodimers have proven to be an efficient drug target for cancer therapy. A broad range of agents, including **ELR510444** and parbendazole, can bind to tubulin and interfere with microtubule assembly. **ELR510444** and parbendazole are colchicine binding site inhibitors with antiproliferative activities. However, the lack of structural information on the tubulin–**ELR510444**/parbendazole complex has hindered the design and development of more potent drugs with similar scaffolds. Therefore, we report the crystal structures of tubulin complexed with **ELR510444** at a resolution of 3.1 Å and with parbendazole at 2.4 Å. The structure of these complexes revealed the intermolecular interactions between the two colchicine binding site inhibitors and tubulin, thus providing a rationale for the development of novel benzsulfamide and benzimidazole derivatives targeting the colchicine binding site.

Introduction

Microtubles, a key component of the eukaryotic cytoskeleton, are cylindrical molecules consisting of two subunits: α-tubulin and β-tubulin. It is known that α/β-tubulin heterodimers can be assembled into protofilaments with a head-to-tail formation, characterized by dynamic polymerization and depolymerization. Microtubules are involved in cell division, in which mitosis, morphogenesis, motility, and intracellular transport occur.[1] In addition, microtubules have been reported to participate in the proliferation, invasion, and metastasis of tumor cells. In recent years, microtubules have been regarded as an important target for oncotherapy. At present, microtubule inhibitors, which disrupt microtubule dynamics, are used widely in cancer chemotherapy.[2] Most of these molecules act by binding to the protein tubulin.[3–8] There are several binding sites on the tubulin heterodimer, including for vinca alkaloids, taxanes, colchicine, and laulimalide,[8] which are usually divided into two categories: microtubule stabilizers, including taxanes and laulimalide, which enhance tubulin polymerization; and microtubule depolymerizers, including vinca alkaloids and colchicine binding site agents, which inhibit tubulin polymerization. The microtubule destabilizers currently in clinical use include vinca alkaloids, vinblastine, vincristine, and vinorelbine, all of which bind to what has been termed the "vinca site" on tubulin. Another recognized binding site for microtubule-destabilizing agents is the colchicine binding site (CBS). Antitubulin agents are currently employed in cancer treatment. However, drug resistance arising from MDR1 expression in cancer cells leads to treatment failure. One drawback of microtubule-targeting agents is drug resistance, which can be innate or acquired. The most common form of clinical resistance to microtubule-targeting agents is overexpression of the *MDR1* gene, which encodes the *P*-glycoprotein (*Pgp*) drug efflux pump.[9] The other clinically relevant form of resistance to microtubule-targeting agents is overexpression of the type III isotype of tubulin.[10] Extensive research has indicated that tubulin inhibitors targeting the CBS are candidate compounds to overcome the limitations of drug resistance and improve the associated clinical benefit.[11,12]

ELR510444, a sulfonamide derivative, was reported to inhibit tubulin polymerization, causing a loss of cellular microtubules (EC50 = 21 nM) and the formation of aberrant mitotic spindles, which led to mitotic arrest and apoptosis in cancer cells; in addition, significant antitumor activity was observed in the

[a]*Cancer Center, West China Hospital, Sichuan University, Collaborative Innovation Center of Biotherapy, Chengdu 610041, P. R. China. E-mail: yuxiwang@scu.edu.cn*

[b]*Targeted Tracer Research and Development Laboratory, Precision Medicine Research Center, Department of Respiratory and Critical Care Medicine, West China Hospital, Sichuan University, Chengdu 610041, P. R. China*

[c]*Department of Clinical Research, West China Hospital Sichuan University, Chengdu 610041, P. R. China*

[d]*Beijing Loham Co.,Limited, Beijing 100068, P. R. China*

[e]*Department of Pharmaceutical Sciences, College of Pharmacy, University of Tennessee Health Science Center, Memphis, Tennessee 38163, USA*

[f]*West China National Clinical Research Center for Geriatrics, School of Nursing, Sichuan University, Chengdu 610041, P. R. China. E-mail: 520067015@qq.com*

† Electronic supplementary information (ESI) available. See DOI: 10.1039/d1ra01173a

‡ These authors contributed equally to this work.

MDA-MB-231 xenograft model.[13] Carew *et al.* reported that **ELR510444** inhibits tumor growth and angiogenesis by abrogating HIF activity and disrupting microtubules in renal cell carcinoma.[14] Extensive studies have indicated that **ELR510444** is not a substrate for the *Pgp* drug transporter and retains activity in β III-tubulin-overexpressing cell lines, suggesting that it avoids both the clinically relevant mechanisms of resistance to this class of agents.[13] However, the binding mode between **ELR510444** and tubulin remains unclear. In addition, another chemotype of CBS inhibitors (CBSIs), benzimidazole carbamates, has been shown to inhibit the assembly of mammalian brain microtubules *in vitro*. Parbendazole was reported to be a potent inhibitor of microtubule assembly *in vitro* and *in vivo*, and was more effective than nocodazole.[15,16] In a panel of four tested benzimidazoles, parbendazole exhibited the strongest antiproliferative activities against AsPC-1 (IC_{50} = 0.19 μM) and Capan-2 cells (IC_{50} = 0.36 μM), indicating its antitumor potential.[17] Parbendazole binds to the tubulin dimer with a 1 : 1 stoichiometry, and microtubules were reported to withdraw from the cell periphery within 30 min after treatment with parbendazole.[15] We previously reported the crystal structure of the nocodazole–tubulin complex and revealed that nocodazole was bound deep within the CBS.[18] However, the reason for the greater potency of parbendazole remains unknown.

To increase the efficacy of inhibition, it is necessary to explore the binding mode between **ELR510444** and tubulin, which will facilitate subsequent structural optimization. To better understand the structure–activity relationship (SAR), and provide a solid structural basis for the development of novel benzimidazole derivatives, we also need to solve the structure of the parbendazole–tubulin complex.

Experimental methods

Special reagents

Porcine brain tubulin (catalog#: T-238P) was purchased from Cytoskeleton. The tubulin protein was supplied at 10 mg mL^{-1} in G-PEM (general tubulin buffer: 80 mM PIPES pH 6.9, 2 mM $MgCl_2$, 0.5 mM EGTA, 1 mM GTP) as a frozen liquid and stored at −80 °C until use. **ELR510444** and parbendazole were purchased from MedChem Express. All reagents for crystallization (MES, tyrosine, DTT, and AMPPCP) were purchased from Sigma.

Protein expression and purification

The stathmin-like domain of RB3 (RB3-SLD) and tubulin tyrosine ligase (TTL) were overexpressed in *E. coli* strain BL21 (DE3). RB3-SLD was purified by anion-exchange chromatography (loading buffer: 20 mM Tris–HCl pH 8.0, 1 mM EGTA, 2 mM DTT; elution buffer: 20 mM Tris–HCl pH 8.0, 1 mM EGTA, 2 mM DTT, 2 M NaCl) and gel filtration chromatography (buffer: 10 mM HEPES pH 7.2, 150 mM NaCl, 2 mM DTT). The peak fractions from the gel filtration column were concentrated to 10 mg mL^{-1}. TTL was purified through Ni-NTA affinity chromatography and gel filtration chromatography (buffer: bis–tris propane pH 6.5, 200 mM NaCl, 2.5 mM $MgCl_2$, 5 mM DTT). The peak fractions of TTL were concentrated to 20 mg mL^{-1}. All proteins were stored at −80 °C.

In vitro tubulin binding

Binding affinity with tubulin was analyzed using surface plasmon resonance (SPR) technology in a Reichert 4SPR system (Reichert Technologies, Depew, NY) equipped with a SPR sensor chip HC 1500 M. First, 50 μg mL^{-1} tubulin (Cytoskeleton, T-238P) was immobilized to the sensor chip surface to attain 10, 000 RU. One of the four flow channel on the chip was left free as a blank control. **ELR510444**, parbendazole or colchicine at different concentrations was injected over the sensor chip surface for association analysis, followed by dissociation analysis. The experiment data were obtained at 25 °C with running buffer PBST (8 mM Na_2HPO_4, 136 mM NaCl, 2 mM KH_2PO_4, 2.6 mM KCl, and 0.05% (v/v) Tween 20, pH 7.4). The equilibrium dissociation constant (K_D) was calculated by a steady-state fitting mode with TraceDrawer software.

Crystallization and crystal soaking

Crystals of T2R-TTL complex (α/β tubulin, RB3-SLD, TTL) were cultivated by the sitting drop vapor diffusion method at 20 °C; details of the process have been reported previously.[19] Briefly, the protein complex (α/β tubulin, RB3, and TTL at a 2 : 1.3 : 1.2 molar ratio) was incubated on ice with 1 mM AMPPCP, 5 mM tyrosine, and 10 mM DTT for 30 min, and the complex was then concentrated to 20 mg mL^{-1} at 4 °C. A drop of solution, consisting of 1 μL of the protein complex and 1 μL of crystallization buffer (6% PEG 4000, 5% glycerol, 100 mM MES pH 6.7, 30 mM $CaCl_2$, 30 mM $MgCl_2$), was placed in each well. Seeding was performed to improve the quality of crystals. The first crystals

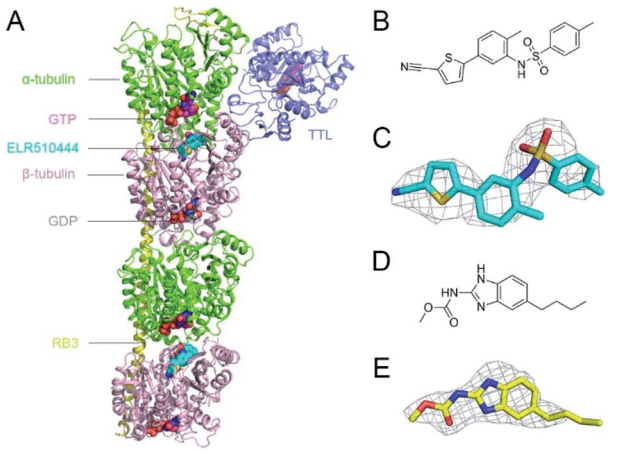

Fig. 1 Overview of the T2R-TTL-ligand complex structure and the chemical structures of the bound ligands. (A) Overall structure of the tubulin–**ELR510444** complex. RB3-SLD is shown in yellow, TTL in blue, α-tubulin in green, β-tubulin in pink, GTP in red, GDP in grey, and **ELR510444** in cyan. GTP, GDP, and **ELR510444** are shown as spheres. (B) Chemical structure of **ELR510444**. (C) Experimental electron density map (Fo–Fc) contoured at 2.0 σ around **ELR510444**. (D) Chemical structure of parbendazole. (E) The electron densities of parbendazole. The Fo–Fc omit map is shown in grey and contoured at 1.5 σ.

appeared after 2 days, and reached their final size within 3–5 days. Different concentrations of **ELR510444** and parbendazole were dissolved in 10 mM DMSO, and the crystals were soaked with each compound (0.1 μL) at 20 °C for 24 h. Crystals with a good shape were picked and snap-frozen in liquid nitrogen with a cryoprotectant (100 mM MES pH 6.7, 30 mM $CaCl_2$, 30 mM $MgCl_2$, 20% glycerine).

Data collection and structure determination

The crystals of the T2R-TTL-**ELR510444**/parbendazole complexes were mounted in nylon loops and flash-cooled in a cold nitrogen stream at 100 K. Diffraction data were collected at the Shanghai Synchrotron Light Source (Shanghai, China); the data were indexed, integrated, and scaled using HKL2000.[20] Structures were solved by molecular replacement with Phaser[21] using the T2R-TTL structure (PDB ID: 4I55) as the template. The initial models were refined by alternating cycles of automatic refinement with Refmac5 (ref. 22) in the CCP4 program suite and manual model building with Coot.[23] The quality of the model was checked with the PROCHECK program, and showed good stereochemistry according to the Ramachandran plot.[24] PYMOL (http://www.pymol.org) was used to generate the figures.

Table 1 Data collection and refinement statistics for X-ray structures[a]

Parameters	Tubulin/**ELR510444**	Tubulin/parbendazole
PDB ID	7DBD	7DBC
Data collection		
Space group	$P2_12_12_1$	$P2_12_12_1$
Cell dimension		
a, *b*, *c* (Å)	104.6	105.4
	158.3	158.3
	182.3	180.8
α, *β*, *γ* (°)	90	90
	90	90
	90	90
Resolution (Å)	49.87–3.1 (3.2–3.1)	19.91–2.4 (2.49–2.4)
R_{merge}	0.303 (1.0)	0.104 (0.772)
I/sigma	8.7 (1.8)	10.3 (2.2)
Completeness (%)	100 (100)	99.8 (100)
Redundancy	12.8 (12.5)	6.8 (6.7)
Refinement		
No. of unique	54 906	118 342
Reflections $^{R}_{work}/^{R}_{free}$ (%)	19.10/24.40	19.79/23.37
No. of atoms	17 563	17 950
Protein	17 332	17 327
Ligand	231	192
Water	—	431
***B*-Factors (Å)**		
Protein	62.90	56.56
Ligand	63.42	54.64
Water	—	49.23
RMS bond length (Å)	0.01	0.01
RMS bond angle (°)	1.30	1.06
Ramachandran plot statistics		
Most favorable (%)	94.41	96.95
Allowed (%)	5.59	3.05
Outliers (%)	0	0

[a] Data for the highest resolution shell are shown in parentheses.

Molecular docking

The receptor was extracted from the solved structure of the **ELR510444**–tubulin complex. The macromolecule and 24

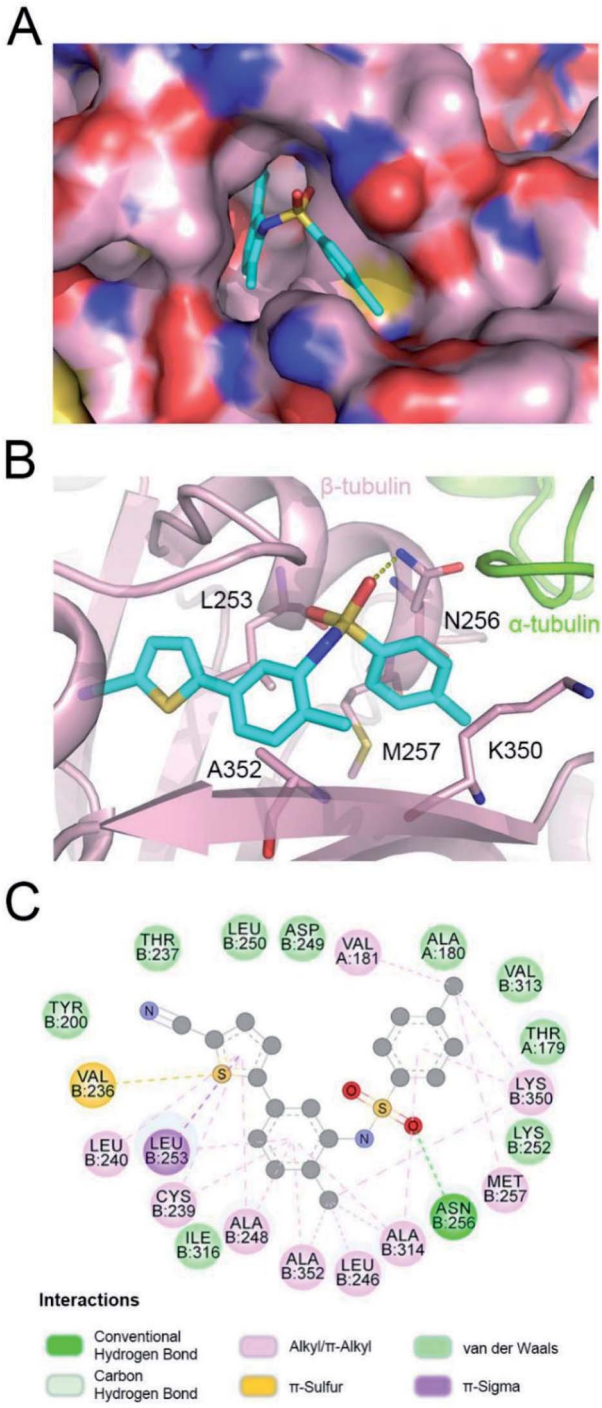

Fig. 2 Detailed interactions of **ELR510444** with tubulin. Surface view of the **ELR510444**–tubulin complex (A) and intermolecular interactions of the binding (B). (C) Two-dimensional interaction map of the **ELR510444** complex with β-tubulin.

inhibitors were then prepared using AutoDockTools.[25] Each inhibitor was docked into the CBS by AutoDock Vina.[26] The docking search space was a rectangular parallelepiped, 16 × 16 × 20 points in size, with a spacing of 1 Å. The exhaustiveness parameter was set to 12.

Results and discussion

In this study, we obtained X-ray crystal structures of **ELR510444** or parbendazole binding to tubulin. **ELR510444** or parbendazole was soaked in a protein complex composed of α/β-tubulin, RB3-SLD, and TTL. We determined the complex structure at a resolution of 3.1 Å for **ELR510444** (Fig. 1A) and 2.4 Å for parbendazole. Details of the data collection and refinement statistics are summarized in Table 1. The structures of **ELR510444** and parbendazole are shown in Fig. 1B and D, respectively. The two inhibitors were well defined by electron density, allowing us to analyze the molecular interactions unambiguously (Fig. 1C and E).

Structure of ELR510444–tubulin complex

In the tubulin–**ELR510444** crystal complex, **ELR510444** occupied the CBS (Fig. 2A). As shown in Fig. 2A and B, the *p*-toluene sulfonamide group of **ELR510444** was buried in a channel surrounded by the N256, M257, and K350 residues of β-tubulin.

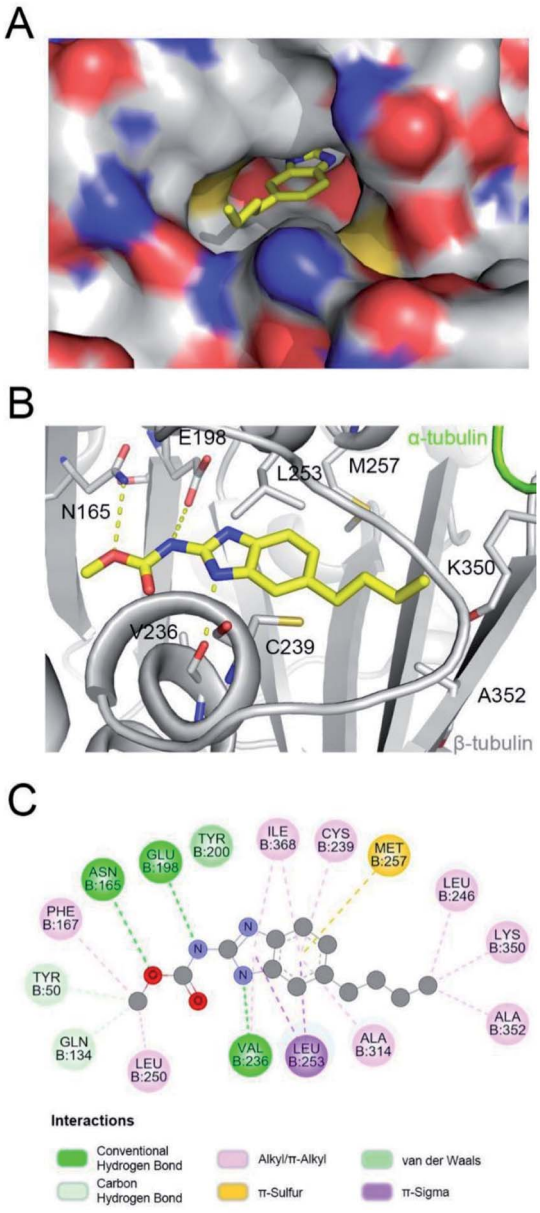

Fig. 3 Detailed interactions of parbendazole with tubulin. Surface view of the parbendazole–tubulin complex (A) and intermolecular interactions of the binding (B). (C) Two-dimensional interaction map of parbendazole complexes with β-tubulin.

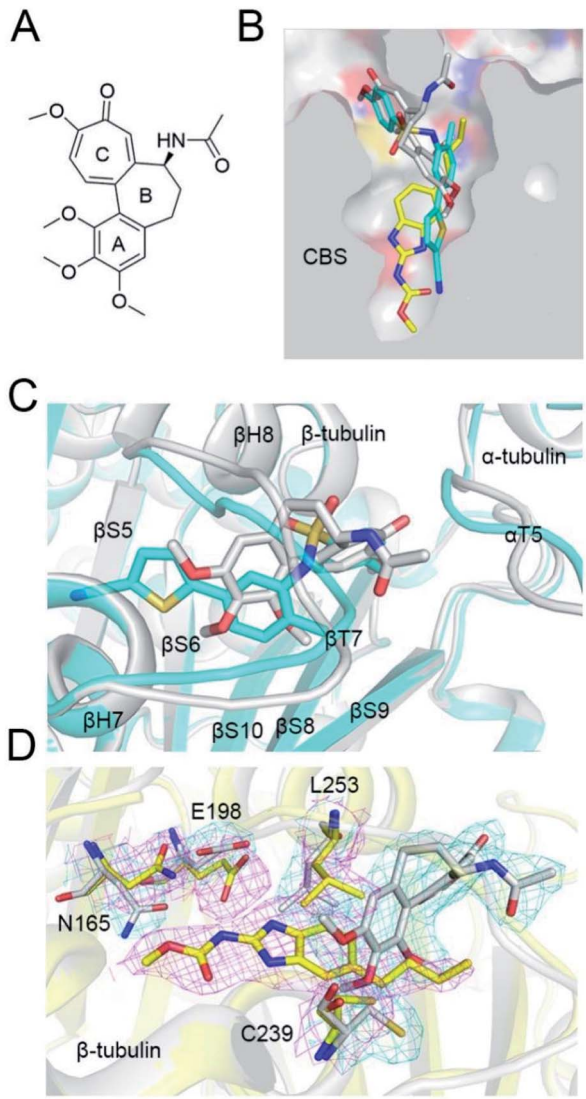

Fig. 4 Comparison of the binding modes of **ELR510444**, parbendazole, and colchicine. (A) Chemical structure of colchicine. (B) Superimposition of β-tubulin binding with **ELR510444** (cyan sticks), parbendazole (yellow sticks), and colchicine (grey sticks) in CBS. (C) Conformation of the αT5 and βT7 loops differs significantly when **ELR510444** or colchicine is bound. (D) Superimposition of parbendazole and colchicine. Residues with significant differences in conformation are highlighted with 2Fo–Fc map contours.

The thiophene-2-carbonitrile moiety was inserted deeply into the colchicine binding cavity. The sulfamide oxygen formed a hydrogen bond with the side chain of N256. As shown in Fig. 2C, there were extensive hydrophobic interactions between **ELR510444** and β-tubulin, including at residues C239, L240, L246, A248, L253, A314, K350, and A352.

Structure of parbendazole–tubulin complex

Parbendazole inserted straight and deeply into the CBS (Fig. 3A). The carbamate group was located at the bottom of the cavity and formed hydrogen bonds with the side chains of N165 and E198. The imidazole formed an additional hydrogen bond with the backbone carbonyl of the V236 residue. The butylbenzene moiety of parbendazole occupied a hydrophobic cavity formed by C239, L246, L253, M257, A314, K350, A352, and I368 (Fig. 3B and C). However, the hydrophobic channel surrounded by the N256, M257, and K350 residues remained unoccupied.

Comparison of ELR510444, parbendazole, and colchicine binding

The colchicine site is a large pocket surrounded by two α-helices (H7 and H8) and strands of the two tubulin β-sheets (S1–S4–S5–S6 and S7–S10–S8–S9), which are from the β subunit and capped by two loops (βT7 and αT5). To compare the tubulin binding mode of **ELR510444** and parbendazole with that of colchicine, we superimposed the two tubulin–CBSI structures onto the tubulin–colchicine structure (PDB ID: 4O2B), revealing that the toluene ring of **ELR510444** superimposed well with the C-ring of colchicine. **ELR510444** binds a little more deeply with β-tubulin than colchicine (Fig. 4B). The conformations of the two capped loops βT7 and αT5 differ significantly, indicating the flexibility required to accommodate the diverse structures of the CBSIs (Fig. 4C). Nevertheless, parbendazole is buried more deeply in β-tubulin (Fig. 5B). Unlike colchicine, parbendazole has no interaction with α-tubulin. Four residues (N165, E198, C239, L253) adopted very different conformations after parbendazole or colchicine binding (Fig. 4D). Interestingly, the binding affinity of the 3 CBSIs to β-tubulin seems to be correlated with the inserting depth in the CBS. The deeper inserted, the tighter binding to tubulin. Three hydrogen bonds and hydrophobic interactions also probably contribute to the higher binding affinity of parbendazole (K_D = 3.39 μM) than that of **ELR510444** (K_D = 22.6 μM) and colchicine (K_D = 28.1 μM) (ESI Fig. S1†).

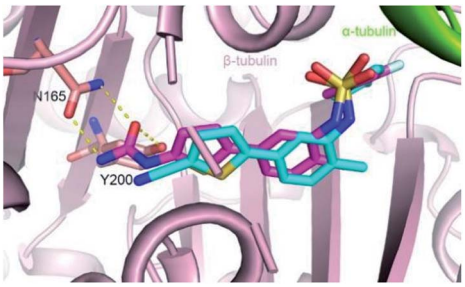

Fig. 5 Alignment of ELR510444 and C22. ELR510444 (cyan sticks) was copied from the crystal structure, whereas C22 (magenta sticks) was docked into the CBS by Autodock Vina. Interactions between C22 and β-tubulin differing from that of ELR510444 are highlighted by yellow dashed lines.

Insights into drug design and molecular docking

CBSIs are a class of structurally diverse agents. **ELR510444** and parbendazole are CBSIs, and both showed inhibition of microtubule assembly. The binding modes identified in this work should allow subsequent structural optimization that will improve the potency of inhibition and reduce side effects. **ELR510444** and parbendazole were located at the CBS. **ELR510444** was bound a little deeper within the CBS than colchicine and made hydrophobic contacts with Val181 of α-tubulin. Parbendazole was located deep within the β subunit and did not interact with the α subunit. Consistent with our previous study,[18] the two loops (T5 of the α subunit and T7 of the β subunit) capped the colchicine domain and adjusted their conformations to accommodate the diverse structures of the CBSIs (Fig. 4B).

ELR510444 almost fully occupied the CBS, except the bottom of the pocket. A cyano group was located at the bottom of the binding pocket. Here, the cyano group could be extended to interact with Asn165. Since computer-aided drug design plays an important role in drug discovery,[27] we also conducted molecular docking experiments on this tubulin complex. A series of **ELR510444** derivatives with different substituents was designed and docked into the CBS by Autodock Vina.[25] These compounds and their predicted binding affinities are listed in

Table 2 Predicted binding affinities of designed compounds

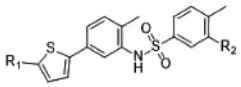

Compound	R_1	R_2	Affinity (kcal mol^{-1})
ELR510444	CN	H	−11.1
C1	CF_2	H	−11.0
C2	CF_3	H	−11.2
C3	CH_2CH_3	H	−10.5
C4	CH_2OH	H	−10.6
C5	CH_2NHCH_3	H	−10.1
C6	$CONHCH_3$	H	−11.0
C7	CCH	H	−11.3
C8	$CCCH_3$	H	−11.2
C9	$CHCH_2$	H	−10.6
C10	$CH(CH_2)_2$	H	−11.0
C11	CH_2CONH_2	H	−11.2
C12	$OCONH_2$	H	−11.0
C13	NHCOH	H	−10.6
C14	$NHCOCH_3$	H	−11.3
C15	$NHCONH_2$	H	−11.5
C16	$NHCOOCH_3$	H	−10.9
C17	$NHSO_2CH_3$	H	−10.4
C18	SO_2NH_2	H	−10.5
C19	CN	F	−11.2
C20	CN	Cl	−10.5
C21	CN	CH_3	−10.9
C22	$NHCONH_2$	F	−11.7

Table 2. **ELR510444** had a strong binding affinity (-11.1 kcal mol^{-1}). Compounds with substituents such as alkynyl (**C7**), formamido (**C14**), and urea (**C15**) groups at the R_1 position had stronger binding affinities than **ELR510444**, whereas a hydrogen at the R_2 position was preferentially displaced by fluorine (**C19**). With both the best predicted R_1 and R_2 substituents, compound **C22** exhibited superior binding affinity (-11.7 kcal mol^{-1}) compared with other **ELR510444** derivatives. In addition, the predicted binding pose of **C22** almost overlapped with **ELR510444** (Fig. 5), indicating the reliability of the docking results.

Parbendazole was the most effective among the series of benzimidazole derivatives, including nocodazole, fenbendazole, mebendazole, and oxibendazole,[17] indicating that the *n*-5-butyl group was preferred to the 2-acetylthiophene, phenyl, and propyl groups. Nocodazole and parbendazole have a same benzimidazole core with different hydrophobic substituents on the phenyl ring. It is a thiophene-2-carbonyl group for nocodazole while an *n*-butyl for parbendazole. Both two groups laid in a hydrophobic cavity surrounded by L246, L253, A314, I316, A352. *n*-Butyl is more hydrophobic than thiophene-2-carbonyl and be preferred in the cavity, thus explaining the reason of superior inhibitory effect of parbendazole.

Conclusions

We reported the X-ray structure of tubulin in complex with **ELR510444** or parbendazole, and it showed that **ELR510444** and parbendazole occupied the colchicine binding pocket. The structures represented the key interactions between tubulin and ligands, and the high-resolution structure of the tubulin–parbendazole complex facilitated the understanding of previous SARs of benzimidazoles. Structural alignment and molecular docking studies were used to achieve the theoretical structural optimization of **ELR510444** and parbendazole. The docking results indicated that substitutions on the thienyl (R1) or phenyl (R2) groups of **ELR510444** were compatible with binding to tubulin. Collectively, our results provide a solid foundation for the development of novel benzsulfamide and benzimidazole derivatives targeting the colchicine binding site, which will support further structural optimization.

Funding

This work was supported by National Natural Science Foundation of China (82073318, 81703553), National Major Scientific and Technological Special Project for 'Significant New Drugs Development' (2018ZX09201018-021), Sichuan Science and Technology Program (2019YFS0003), China Postdoctoral Science Foundation (2018T110984, 2017M610607), and Post-Doctoral Research Project, West China Hospital, Sichuan University (2018HXBH057).

Data availability

The atomic coordinates and structure factors for tubulin–CBSI complexes have been deposited in the Protein Data Bank under accession codes 7DBD (tubulin–**ELR510444**) and 7DBC (tubulin–parbendazole).

Author contributions

Conceptualization: Yu-Xi Wang; data curation: Jing-Hong Xian and Hai Chen; formal analysis: Yu-Yan Li; funding acquisition: Yu-Xi Wang; investigation: Ling-Ling Ma and Jia-Hong Lei; methodology: Jia-Hong Lei, Ling-Ling Ma and Jian-Jian Zhou; software: Qian Lei and Hai Chen; writing – original draft: Jia-Hong Lei; writing – review & editing: Hao Chen, Yan-Yan Wang, and Yu-Xi Wang. All authors have read and agreed to the published version of the manuscript.

Conflicts of interest

There are no conflicts to declare.

Acknowledgements

The authors thank the staff from the BL17U1, BL18U1, BL19U1 beamlines of the National Facility for Protein Science Shanghai (NFPS) at Shanghai Synchrotron Radiation Facility for assistance with data collection.

Notes and references

1 E. Nogales, *Annu. Rev. Biophys. Biomol. Struct.*, 2001, **30**, 397–420.
2 C. Dumontet and M. A. Jordan, *Nat. Rev. Drug Discovery*, 2010, **9**, 790–803.
3 E. C. McLoughlin and N. M. O'Boyle, *Pharmaceuticals*, 2020, **13**, 8.
4 M. O. Steinmetz and A. E. Prota, *Trends Cell Biol.*, 2018, **28**, 776–792.
5 W. Li, H. Sun, S. Xu, Z. Zhu and J. Xu, *Future Med. Chem.*, 2017, **9**, 1765–1794.
6 X. Wu, Q. Wang and W. Li, *Anti-Cancer Agents Med. Chem.*, 2016, **16**, 1325–1338.
7 M. J. Perez-Perez, E. M. Priego, O. Bueno, M. S. Martins, M. D. Canela and S. Liekens, *J. Med. Chem.*, 2016, **59**, 8685–8711.
8 Y. Lu, J. Chen, M. Xiao, W. Li and D. D. Miller, *Pharm. Res.*, 2012, **29**, 2943–2971.
9 T. Fojo and M. Menefee, *Ann. Oncol.*, 2007, **18**(suppl. 5), v3–8.
10 P. Seve and C. Dumontet, *Lancet Oncol.*, 2008, **9**, 168–175.
11 K. E. Arnst, Y. Wang, D. J. Hwang, Y. Xue, T. Costello, D. Hamilton, Q. Chen, J. Yang, F. Park, J. T. Dalton, D. D. Miller and W. Li, *Cancer Res.*, 2018, **78**, 265–277.
12 C. Stengel, S. P. Newman, M. P. Leese, B. V. Potter, M. J. Reed and A. Purohit, *Br. J. Cancer*, 2010, **102**, 316–324.
13 A. L. Risinger, C. D. Westbrook, A. Encinas, M. Mulbaier, C. M. Schultes, S. Wawro, J. D. Lewis, B. Janssen, F. J. Giles and S. L. Mooberry, *J. Pharmacol. Exp. Ther.*, 2011, **336**, 652–660.

14 J. S. Carew, J. A. Esquivel III, C. M. Espitia, C. M. Schultes, M. Mulbaier, J. D. Lewis, B. Janssen, F. J. Giles and S. T. Nawrocki, *PLoS One*, 2012, **7**, e31120.
15 C. M. Ireland, K. Gull, W. E. Gutteridge and C. I. Pogson, *Biochem. Pharmacol.*, 1979, **28**, 2680–2682.
16 J. C. Havercroft, R. A. Quinlan and K. Gull, *J. Cell Sci.*, 1981, **49**, 195–204.
17 R. Florio, S. Veschi, V. di Giacomo, S. Pagotto, S. Carradori, F. Verginelli, R. Cirilli, A. Casulli, A. Grassadonia, N. Tinari, A. Cataldi, R. Amoroso, A. Cama and L. De Lellis, *Cancers*, 2019, **11**, 2042.
18 Y. Wang, H. Zhang, B. Gigant, Y. Yu, Y. Wu, X. Chen, Q. Lai, Z. Yang, Q. Chen and J. Yang, *FEBS J.*, 2016, **283**, 102–111.
19 J. Yang, Y. Wang, T. Wang, J. Jiang, C. H. Botting, H. Liu, Q. Chen, J. Yang, J. H. Naismith, X. Zhu and L. Chen, *Nat. Commun.*, 2016, **7**, 12103.
20 Z. Otwinowski and W. Minor, *Methods Enzymol.*, 1997, **276**, 307–326.
21 A. J. McCoy, R. W. Grosse-Kunstleve, P. D. Adams, M. D. Winn, L. C. Storoni and R. J. Read, *J. Appl. Crystallogr.*, 2007, **40**, 658–674.
22 G. N. Murshudov, P. Skubak, A. A. Lebedev, N. S. Pannu, R. A. Steiner, R. A. Nicholls, M. D. Winn, F. Long and A. A. Vagin, *Acta Crystallogr., Sect. D: Biol. Crystallogr.*, 2011, **67**, 355–367.
23 P. Emsley and K. Cowtan, *Acta Crystallogr., Sect. D: Biol. Crystallogr.*, 2004, **60**, 2126–2132.
24 R. A. Laskowski, J. A. Rullmann, M. W. MacArthur, R. Kaptein and J. M. Thornton, *J. Biomol. NMR*, 1996, **8**, 477–486.
25 G. M. Morris, R. Huey, W. Lindstrom, M. F. Sanner, R. K. Belew, D. S. Goodsell and A. J. Olson, *J. Comput. Chem.*, 2009, **30**, 2785–2791.
26 O. Trott and A. J. Olson, *J. Comput. Chem.*, 2010, **31**, 455–461.
27 X. Chang, D. Sun, D. Shi, G. Wang, Y. Chen, K. Zhang, H. Tan, J. Liu, B. Liu and L. Ouyang, *Acta Pharm. Sin. B*, 2021, **11**, 156–180.